JOURNAL OF GEOPHYSICAL RESEARCH, VOL. 104, NO. E7, PAGES 16,515–16,529, JULY 25, 1999

Gruithuisen domes region: A candidate for an extended nonmare volcanism unit on the Moon

Serge D. Chevrel and Patrick C. Pinet
Laboratoire de Dynamique Terrestre et Planétaire (UMR5562/CNRS/Université Paul Sabatier), Groupe de Recherche de Geodésie Spatiale, Observatoire Midi-Pyrénées, Toulouse, France.

James W. Head
Department of Geological Sciences, Brown University, Providence, Rhode Island.

Abstract. Small lunar areas known as red spots are thought to represent good candidates for nonmare volcanic units predating or contemporaneous with the period of mare volcanism. In this study, we present imaging telescopic and orbital Clementine multispectral surveys of the Gruithuisen region, located in the northwestern border of Mare Imbrium, which contains Imbrian age domical features of likely viscous volcanic origin with spectral characteristics of red spot areas. A rather spectrally homogeneous unit having typical characteristics of red spots is found to coincide with the material within the morphological boundaries of the Gruithuisen Delta, Gamma and Northwest domes. An extended "dome-like" unit is identified spectrally and surrounds and extends to the west and the north of the domes. This unit shows spectral characteristics close to those of the domes, suggesting the presence of a significant amount of dome material extending many kilometers away from the domes themselves. Both the spectral characteristics of the dome and the dome-like unit are clearly different from those of highlands and the surrounding mare basalts. The spectral identification of a widespread dome-like unit suggests that the specific style of eruption that is inferred for the formation of the domes (i.e., viscous flows of possible more silicic composition) might have occurred on a regional scale in this part of the Moon, prior to the Iridum event about 3.8 Gyr ago. This volcanic style appears to be more widespread in the early part of lunar history than previously thought.

1. Introduction

With few exceptions, the volcanic activity on the Moon is viewed in terms of mare volcanism only because of the widespread evidence of mare basalt deposits on the lunar surface. The area of exposed mare deposits covers about 17% of the total lunar surface [*Head*, 1976]. Most of the mare volcanism activity occurred during the Imbrian period (3.8-3.2 Ga) [*Wilhelms*, 1987; *Head and Wilson*, 1992]. However, there is evidence that the lunar mare volcanism was an ongoing process in the early Imbrian, Nectarian, and perhaps pre-Nectarian periods, i.e., prior to the termination of late heavy bombardment [*Schultz and Spudis*, 1979; *Hawke and Bell*, 1981; *Hartmann et al.*, 1981]. The recognition of deposits known as cryptomare (mare basalt deposits mixed with and covered by higher albedo basin and crater ejecta of the highland crust) [e.g., *Head et al.*, 1993; *Greeley et al.*, 1993] has increased the total area covered by mare deposits by up to 20% of the total lunar surface. On the other end, there is evidence for the duration of mare volcanism beyond the 2.5 Ga age proposed for the youngest Imbrium flows [e.g., *Schultz and Spudis*, 1983]. While lunar mare volcanism appears to be relatively well documented, little is known about the emplacement of lunar nonmare volcanic geologic units before and during the period of mare volcanism. As with mare volcanism, the existence of nonmare volcanism has equally major implications for the thermal history and crustal evolution of the Moon. Small lunar areas known as red spots may represent good candidates for such nonmare volcanic geologic units predating or contemporaneous with the period of mare volcanism [*Wood and Head*, 1975]. These anomalous areas, which are primarily characterized by a relatively high albedo and a strong absorption in the UV relative to the visible, were first recognized from telescopic color difference photography [*Whitaker*, 1972; see also *Bruno et al.*, 1991, Figure 1] and from digital vidicon multispectral imaging [*McCord et al.*, 1976; *Head and McCord*, 1978]. They are located in a variety of geological settings, exhibit a wide range of morphologies (domes, smooth plains units, rugged highland patches) [*Wood and Head*, 1975], and show some spectral variations interpreted as differences in composition [*Müller et al.*, 1986; *Bruno et al.*, 1991]. Many red spots are embayed by younger mare deposits, suggesting that they have originally covered a greater proportion of the lunar surface [*Malin*, 1974].

In this paper, we present imaging telescopic and orbital (Clementine data) multispectral surveys of the Gruithuisen region which contain Imbrian age domical features of likely volcanic origin, having spectral characteristics of red spots areas [*Head and McCord*, 1978; *Chevrel et al.*, 1996]. The present spectral mapping of the Gruithuisen domes region represents an improvement with respect to earlier works where only two reflectance spectra were obtained, that corresponded to portions of the Delta and Gamma domes. The aim of this work is to map in detail the extent of the dome material within

Paper number 1998JE900007.
0148-0227/99/1998JE900007$09.00

the region and to document its relation with the regional spectral units we have identified. In related research, we treat the detailed crater chronology of the Gruithuisen region [*Wagner et al.*, 1996, manuscript in preparation, 1999] and interpreted mineralogy, models for petrogenetic origin, and mode of volcanic emplacement [Head et al., manuscript in preparation, 1999] of the domes and related deposits.

2. Gruithuisen Domes: Geological Setting

The Gruithuisen Delta and Gamma domes are relatively high albedo features located in the northwestern border of Mare Imbrium (36°10'N; 39°20'W and 36°30'N; 40°35'W, respectively), about 250 km south-southwest of Sinus Iridum. They are emplaced on the location of the second ring of the Imbrium multiringed basin. This ring represents the western equivalent of Montes Alpes northeast of Imbrium [*Spudis et al.*, 1988] (Figure 1a). These domical features are topographically distinct from adjacent highland and mare terrains and show unique surface morphology [*Smith*, 1973]. The Gamma dome is a flat-topped feature, roughly circular in shape (about 24 x 18 km at its base), over 1200 m in height (Figures 1b and 1c). The Delta dome is flat-topped, rectangular in outline (about 33 x 13.5 km), and 1500 to 1600 m in height. This dome may be composed of several coalescing domes. A small, roughly circular feature (8 km in diameter and 1100 m in elevation) (Figures 1b and 1c), informally called "Northwest dome" and referred to as NW hereafter, is located northwest of the Gamma dome [*Head and McCord*, 1978; *Head et al.*, 1978]. The flanks of the Gamma dome have slopes ranging from 15° to 30° and show very distinctive texture consisting of ridges and furrows generally oriented downslope [*Schultz*, 1976; *Head and McCord*, 1978]. These morphological and textural characteristics of the Gruithuisen domes are quite different from those of typical domes associated with mare basalts which show a lower albedo, a smaller diameter range and elevation, and smoother surface texture [*Head and Gifford*, 1980].

Earlier reflectance spectra have shown that the Gruithuisen domes are spectrally distinct from the surrounding highland and mare material but are quite similar to high-albedo areas known as red spots [*Head and McCord*, 1978; *Bruno et al.*, 1991]. The Gruithuisen domes thus appear morphologically, texturally, and spectrally distinct from the surrounding mare materials and show no obvious affinities with background highland topography.

Although the morphology and surface texture indicate a volcanic origin for the Gruithuisen domes, their eruption style is distinct from mare basalt eruption styles. The morphology of the flows that are on and surrounding the domes clearly indicates that these flows are highly viscous in their emplacement and may also have been explosive in places [*Head et al.*, 1978]. The Gruithuisen domes are similar in shape and surface texture to many terrestrial domes of dacitic and rhyolitic composition characterized by extrusions of more viscous lavas at low rates. It has been suggested that relatively high silica content and lack of extensive superheating in lunar feldspathic magmas may produce lava of sufficient viscosity to build structures comparable to the Gruithuisen domes [*Head and McCord*, 1978; *Head et al.*, 1978]. The similarities of the Gruithuisen domes Delta and Gamma to terrestrial silicic domes, in terms of morphology and viscosity of lavas, has also led to the interpretation that these features might possibly be related to plutons of more silicic composition than mare basalt that may occur within or below the lunar crust [*Head at al.*, 1978].

Stratigraphic relationships show the Gruithuisen domes appear to have formed early in the Late Imbrian [*Wagner et al.*, 1996]. They postdate the formation of Iridum crater and some mare deposits in the Imbrium and the Procellarum region [*Head and McCord*, 1978]. This suggests that a distinctive style of extrusive nonmare volcanism occurred in this region before and during the early period of mare volcanism. In order to assess the distribution of these units, we have acquired Earth-based telescopic data and we compare it to Clementine multispectral data.

3. Data Acquisition and Processing

Both Earth-based CCD (charge coupled device) images (taken at 2 m aperture (Focal length / Diameter = 25) telescope of the Pic-du-Midi Observatory in France)[*Chevrel et al.*, 1994] and orbital images from the Clementine ultraviolet-visible (UVVIS) multispectral camera [*Nozette et al.*, 1994] are used for complementarity in this study. Telescopic coverage (a single frame, sampling of 0.095 arcsec/pixel, resulting in a 0.9 km/pixel resolution after a binning during the data processing) is centered on the Gruithuisen Delta and Gamma domes. It extends from a mare region located south of the domes to the ejecta blanket of the crater Mairan A to the north, though the crater itself is not included in the image. It includes to the west a portion of the highlands and to the east a portion of the western border of Mare Imbrium, respectively, approximately located between craters Gruithuisen B and Mairan A (see Figures 1 and 2a). The data sets were obtained during the October 1989 full moon period, under 15° of phase angle, and consist of repeated runs comprising eight selected narrowband images at 400, 560, 730, 910, 950, 990, 1020, and 1050 nm (≈100 Å bandwidth). The Clementine mosaic is made by assembling six independent images, obtained at 200 m resolution per pixel. A binning by a factor of 2 results in a mosaic at 400 m/pixel (Figures 1 and 2b). The images were taken through five narrowband (50 to 200 Å bandwidth) filters at 410, 750, 910, 950, and 990 nm, under the same viewing geometry conditions (phase angle, 38-40°; incidence angle 38°-40°; emergence angle, 0°). The telescopic frame is fully included within the Clementine mosaicked image (see Figure 2b).

For the telescopic data set, images in each band have been instrumentally calibrated (i.e. dark field and flat field corrected) and registered, to form an image cube, using procedures described elsewhere [e.g., *Chevrel and Pinet*, 1992]. The Clementine images have been instrumentally calibrated, registered, and mosaicked through the ISIS procedure (version of February 1997) to produce a harmonized mosaic with discrepancies at the overlapping boundaries of the six independent frames, not exceeding 0.5-1.0% for each band. However, during the processing of the Clementine image, we did not apply the photometric model ("moonpr" program) proposed in the ISIS procedure to photometrically adjust the images to a standard viewing geometry of 30° phase angle (i=30°, e=0°)[*McEwen*, 1996]. Indeed, the precise lunar photometric function is not yet fully established for all wavelengths. As a consequence, the level of consistency between the different overlapping frames used when one produces the regional photometric mosaic is still insufficient,

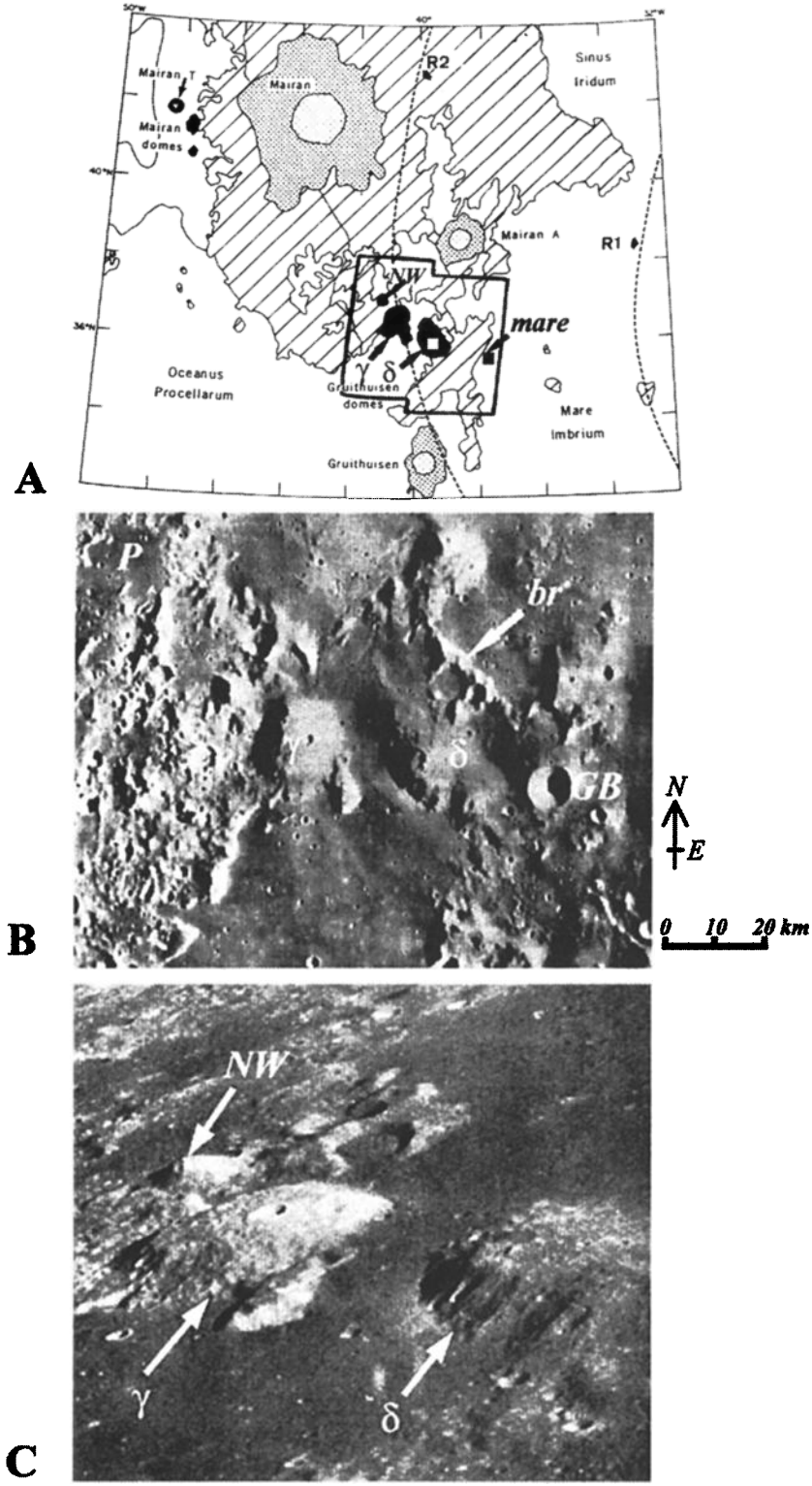

Figure 1. (a) Location and geologic setting of the Gruithuisen Delta, Gamma, and NW domes (shown in black) and coverage of the Clementine mosaic (the telescopic image frame is included within the Clementine mosaic; see Figure 2). Lined areas are high albedo areas previously mapped as highland terrain dominated primarily by Iridum ejecta deposits [*Head and McCord*, 1978]. R1 and R2 mark the location of the inner and intermediate ring, respectively, of the Imbrium basin [*Spudis et al.*, 1988]. The open and solid squares show the location of the Delta Dome and the mare spectra, respectively; used for converting the telescopic and the Clementine image into "absolute" reflectance values. Sketch map is adapted from *Head and McCord*, [1978]. (b) Lunar Orbiter IV image (IV-151-H2) of the Gruithuisen domes region. GB is Gruithuisen B crater, br is branch-shaped massif, and P is mare patch discussed in the text. (c) Oblique view (Apollo 15 image; AS15-12718) of the Gruithuisen domes. North is toward top right, and west is toward left. The top arrow points to the Northwest (NW) dome, while the middle and right arrows point to the Gruithuisen Delta and Gamma domes, respectively (1200 and 1600 m, respectively, in height) [from *Head and McCord* 1978].

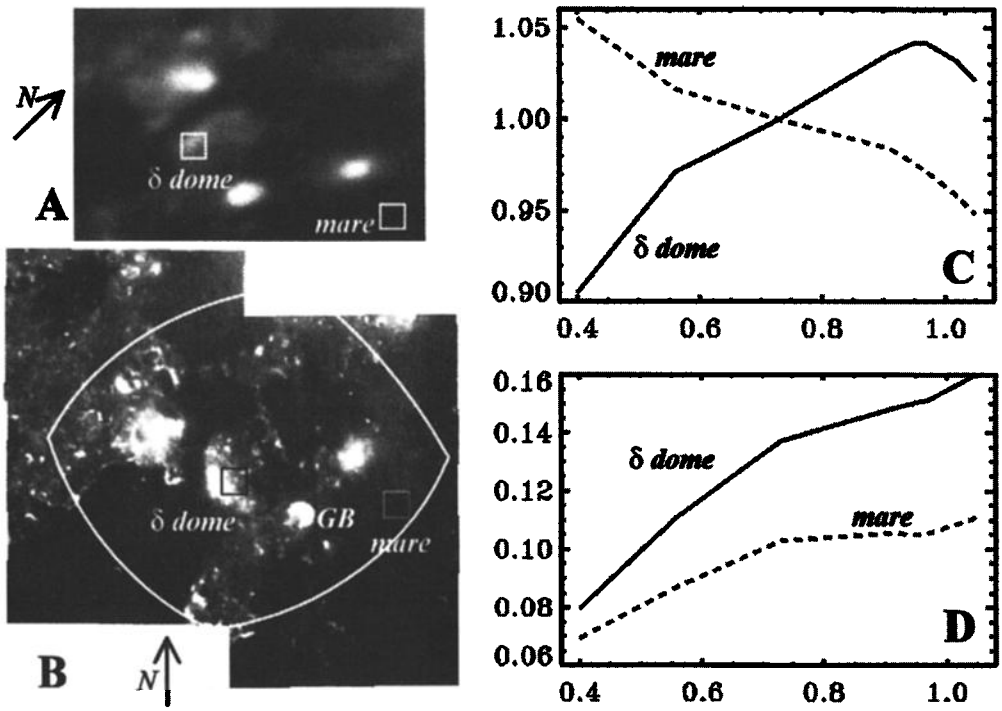

Figure 2. Albedo image at (a) 730 nm and (b) 750 nm from the telescopic and the Clementine data sets. The position of the telescopic frame is shown in Figure 2b. Locations of the Delta Dome and the mare spectra taken as reference and used to calibrate the telescopic and the Clementine image are shown by open squares labeled δ dome and mare, respectively. GB is Gruithuisen B crater. (c) Reflectance spectra relative to MS2 (scaled at 750 nm) taken from *Head and McCord* [1978] (Delta Dome, labeled δ dome) and from *Pieters* [1978] (mare h2 GS-3, labeled mare). (d) Absolute reflectance spectra of the Delta Dome and mare after spectra in Figure 2c are processed using the relationship (equation (1)) given in the text.

and it results in local discontinuities which may reach 3% or more in "absolute" reflectance.

The intended purpose of the present paper is not to propose perfectly corrected data in terms of photometry (which may depend on a number of factors including local topography, surface texture, etc.) but to establish a spectral classification of the region based on a harmonized Clementine mosaic, since statistical techniques used for this matter require a spectral data set with no discontinuities (less than 1% to 2%) for each band between the images comprising the Clementine mosaic. Along with this line of thought and the purpose of interpreting the present new data in the light of earlier data, the Gruithuisen telescopic image and Clementine mosaic have been photometrically calibrated using an empirical line method [*Smith et al.*, 1990a, b], relying on telescopic spectra from previous studies.

Only two spectra located within or in the vicinity of the scene are available from the literature [*Head and McCord*, 1978; *Pieters*, 1978]. These two spectra, which correspond to a dome and a mare area and which are available in the form of relative to MS2 spectra (MS2 is a standard area in Mare Serenitatis, [e.g., *McCord*, 1969]), were corrected to absolute reflectance R (in percent) using the following relationship:

$$[R]_X = [X/\mathrm{MS2}]_i \quad [\mathrm{MS2}/\mathrm{SUN}]_i \quad [A_X]_i \qquad (1)$$

In 1, the first term is the telescopic spectrum of area X relative to MS2 and scaled to unity at the wavelength$i$; the second term is the spectrum of area MS2 versus Sun, scaled to unity at i. The reflectance spectrum MS2 versus Sun is obtained from *Gaddis et al.* [1995]; the third term A is the albedo of area X at the wavelength i. For the telescopic image, i = 560 nm and the albedo A for an area X is taken from *Pohn and Wildey* [1970]. For the Clementine mosaic, i = 750 nm and the albedo is taken from the "Clementine Basemap Mosaic" at 750 nm (A.S. McEwen et al., unpublished data, 1997).

Two areas (labeled "δ dome" and "mare" in Figure 2) that spatially correspond to each other in the telescopic image and the Clementine mosaic and for which a spectrum is available have been taken as reference areas to perform an independent linear regression on both the telescopic image and the Clementine mosaic. These areas correspond to regions of about 9x9 km on the lunar surface (10x10 and 22x22 pixels in the telescopic and the Clementine images respectively)(see Figures 2a and 2b). We have assessed the spectral homogeneity on a regional scale of the chosen location, both in the Clementine and telescopic data sets. The first reference area is a relatively high albedo area located on the southern flank of the Delta dome (36.0°N, 39.5°W)(white square in Figure 1a and open square labeled δ dome in Figures 2a and 2b). The reference spectrum for this area is the Delta dome spectrum versus MS2 (Red spot B/MS2) from *Head and McCord* [1978] (Figure 2c). The second reference area is a low albedo area taken in a mare unit (solid square in Figure 1a and open square labeled mare in Figures 2a and 2b) located east (35.5°N,

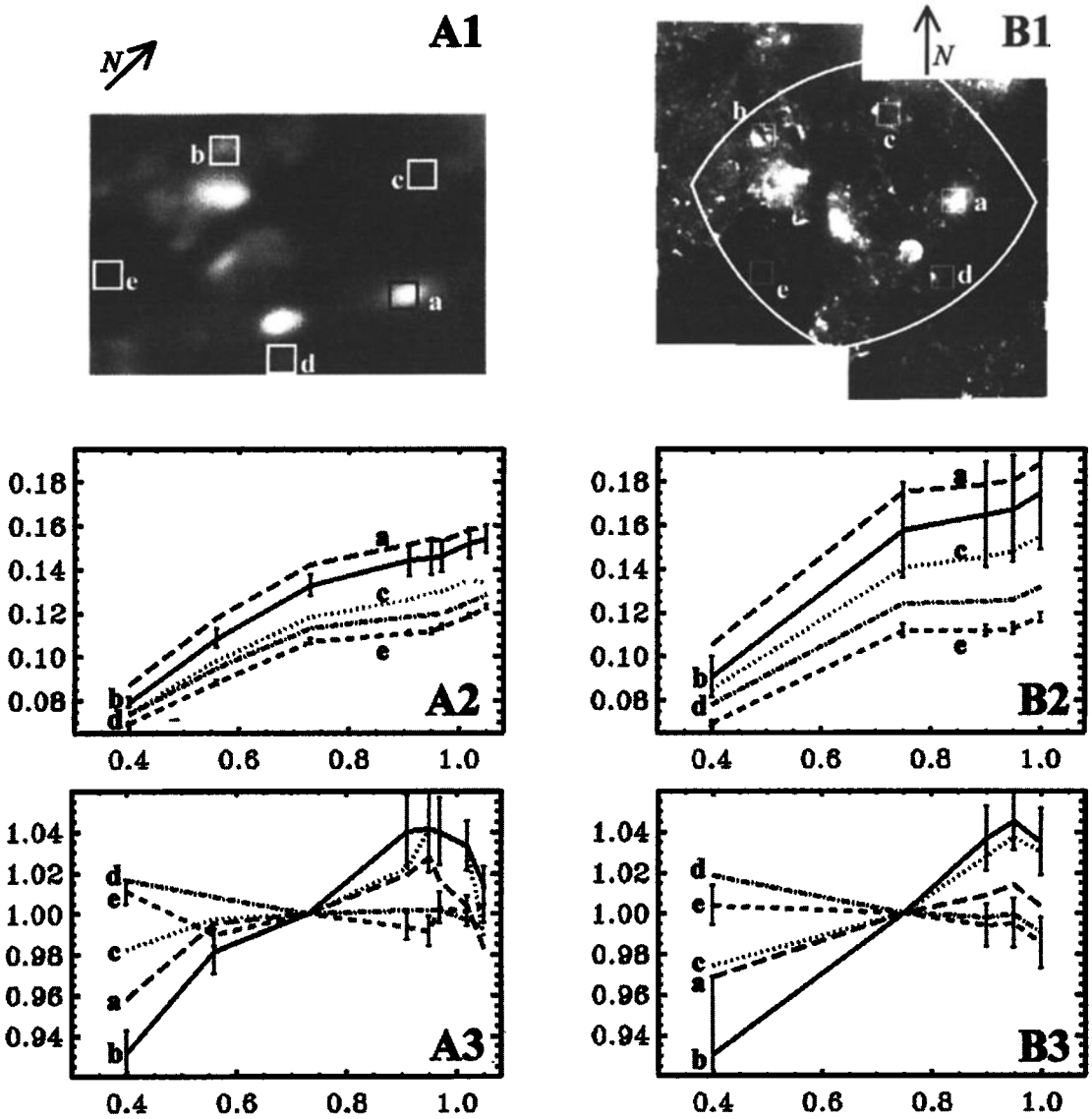

Figure 3. Comparison spectra for the two independent telescopic (A1-A3) and Clementine (B1-B3) data sets. Locations of five spectra (corresponding to high, a and b; intermediate, c; and low, d and e, albedo areas) taken for comparison are shown in the telescopic (A1) and the Clementine (B1) images. Box size is 10x10 pixels in the telescopic image (A1) and 22x22 pixels in the Clementine image (B1), corresponding to 9x9 km areas. Spectra in "absolute" reflectance are shown in A2 for the telescopic and B2 for the Clementine image. Relative MS2 spectra scaled to unity at 730 nm are shown in A3 for the telescopic image and in B3 at 750 nm for the Clementine image.

37°W) of the crater Gruithuisen B (labeled GB in Figure 2b). However, as there is no earlier telescopic mare spectrum available within the image field, we have taken from *Pieters* [1978] a spectrum (h2 GS-3/MS2) located in Mare Imbrium (34.0°N, 25.0°W), close to the crater Carlini (C. M.Pieters, unpublished data, 1976]. According to the TiO_2 abundance map for the nearside maria from *Johnson et al.* [1991a], the h2 GS-3 mare area and the mare area east of Gruithuisen B are located in low-Ti (2-4 wt% TiO_2) mare units which differ by less than 2 wt% in TiO_2 content. Also, an iron abundance map from *Lucey et al.* [1998] indicates that the two mare areas have similar FeO content, ranging from 15 to 20 wt%. These observations are in agreement with other FeO and TiO_2 abundance mapping [e.g., *Kaydash and Shkuratov*, 1998; Y.G. Shkuratov, *personal communication, 1998*]. Finally, according to the spectral mapping of mare basalts by *Pieters* [1978], the two mare areas located east of crater Gruithuisen B (solid square in Figure 1a) and h2 GS-3, close to Carlini, lie in the same spectral unit (refered as hDSA spectral type) [*Pieters*, 1978]. After assessment of their spectral homogeneity at regional scale both in the telescopic and Clementine data sets, it is concluded that the h2 GS-3 mare area and the reference mare area taken east of Gruithuisen B have very close general spectral properties. We then consider the h2 GS-3 spectrum to be representative of the mare area taken as a reference in the Gruithuisen Clementine and telescopic image.

The h2 GS-3 spectrum versus MS2 [*Pieters*, 1978] is shown in Figure 2c. Figure 2d shows the reflectance curves (in five

bands) for the Delta dome and the mare area obtained through (1). These areas are located among the higher and lower albedo areas, respectively, in the image. For the telescopic image, the albedo values at 560 nm for the Delta dome and the mare areas, taken from *Pohn and Wildey* [1970], are 0.110 and 0.087, respectively. The values at 750 nm for the Clementine image, derived from the "Clementine Basemap Mosaic at 750 nm" (A. S. McEwen et al., unpublished data, 1997), are 0.163 and 0.109, respectively. Relying on the Delta dome and mare (h2 GS-3) reflectance spectra (Figure 2d), a linear regression is carried out, and gain and offset values are derived independently for each band of the Clementine and telescopic data sets. This results in two three-dimensional, high quality spectro imaging data sets, with each image pixel characterized by its spectrum ranging from 400 to 1050 nm (telescopic) and 410 to 990 nm (Clementine).

The produced absolute reflectance data may differ from the actual reflectance owing to uncertainties in estimating the albedo areas when producing MS2/Sun. Because of given differences in scale and viewing geometry, the actual reflectance could differ as much as 20% [e.g., see *Pieters et al.*, 1993]. Also, because absolute reflectance achieved through (1) combines both telescopic ("diffuse" or directional hemispheric reflectance) and laboratory (bidirectional reflectance) data [*Pieters et al.*, 1993; *Gaddis et al.*, 1995], which are not related in a linear way, some variations in the spectral slope can be introduced in the resulting spectra. Other slight variations in the spectral slope may also arise from differences in viewing geometry for which the Delta dome and the mare (h2 GS-3) spectra were obtained (phase angle values are about 36° and 25°, respectively). However, it has been shown [*McCord*, 1969] that relative lunar color does not change significantly with phase angle values from 20° to 60°.

Despite these uncertainties, the comparison of spectra taken for small homogeneous areas, corresponding to the same location in both the Clementine and the telescopic image, shows a very good consistency between the two data sets, discrepancies being less than 3-4% in absolute reflectance and less than 1-2% in reflectance relative to MS2. In absolute reflectance, differences occur owing to the different sources, e.g., *Pohn and Wildey* [1970] and A.S. McEwen et al. (unpublished data, 1997), used to retrieve reflectance values of the reference Delta and mare spectra in the telescopic and Clementine data sets, respectively (see above). This good agreement is illustrated in Figure 3, where spectra are shown for five equivalent areas (labeled a-e) in the Clementine and the telescopic image. These areas (9x9 km) have been taken among high (areas a and b), intermediate (area c) and low (areas d and e) albedo units. Spectra are shown in absolute reflectance (labeled A2 and B2 in Figure 3) and in reflectance relative to MS2 (labeled A3 and B3 in Figure 3). Relative to MS2 reflectance, the very good agreement (about 1%) between the two independent data sets gives us a high level of confidence in the spectral variations, i.e., slope changes, which can be observed within the spectra population, both in the Clementine data set (five bands) and in the more spectrally documented telescopic data set (eight bands). It demonstrates that the two independent instrumental calibrations done for the telescopic and Clementine data sets are quite reliable. In the following, a classification is proposed, mainly based on the observation of global changes in the spectral curve, i.e., slope variations in the UV and the near-infrared (NIR) domains, both in absolute and scaled reflectance. Relative reflectance to the lunar standard area MS2 in Mare Serenitatis [*McCord et al.*, 1972; *Pieters*, 1978] is produced because it is widely used in the literature to compare and interpret the spectral properties of lunar terrains.

4. Data Analysis

A multivariate statistical technique of principal component analysis (PCA) [*Davis*, 1973; *Sasaki et al.*, 1983; *Johnson et al.*, 1985, 1994] has been applied to the Gruithuisen telescopic and Clementine spectro imaging data sets (Plate 1). Principal component analysis is an analytical technique based upon a transformation of spectral axes so that variability is maximized. PCA is quite efficient for analysis of remote sensing data for which some channels may be highly correlated, as it permits one to determine the useful dimensionality of the data set and to understand how the data cloud distribution is clustered in factor space. Applied to various geological remote sensing studies [e.g., *Laughlin*,

Plate 1. Clusters and corresponding spatial distribution identified in ^principal component space (PC) within the Gruithuisen domes region in the Clementine mosaic (A1-A5) and telescopic image (B1-B6). Tick bars corresponds to a 1s deviation along the spectral domain for the highest and the lowest spectra (ranging between 1 and 2%). Red represents the dome unit; yellow and orange (only in the telescopic image): dome-like unit; light blue, violet, and dark blue (only in the Clementine image), mare units; and pink and green, areas corresponding to intermediate clusters identified in the PC space (see text). For the sake of clarity, analysis of the Clementine mosaic has been split in two, with a repetition of the spectra associated with the red (dome) and the violet (mare) units. Spatial distribution corresponding to the clusters identified in the PC space, are shown in A1 (Clementine) and B1 (telescopic), while A2 and B2 show mean reflectance spectra corresponding to each cluster for Clementine and telescopic, respectively, selected within the PCA scaled (axes 1 and 2) diagrams in A5 and B5, respectively. A3 (Clementine) and B3 (telescopic) include mean reflectance spectra relative to MS2 corresponding to each spectral domain selected within the PCA scaled (axes 1 and 2) diagram in A5 and B5, respectively. Spectra are scaled to unity at 750 and 730 nm for the Clementine and the telescopic image respectively. The PCA reflectance diagrams are A4 for Clementine and B4 for telescopic and represent the statistical cloud corresponding to the PCA analysis of spectra in "absolute" reflectance. PCA scaled diagram A5 (Clementine) and B5-B6 (telescopic), represent the statistical cloud corresponding to the PCA analysis of spectra in absolute reflectance scaled to unity at 750 nm (Clementine) and 730 nm (telescopic). B6 is after removal of the 1050 nm spectral band (see text). Projection of the cloud is along axis 1 (in abscissa) and axis 2. In both PCA reflectance and PCA scaled diagrams, the point of coordinates (0,0) corresponds to the barycenter point for the population. Arrows in A5 correspond to spectral trends discussed in the text.

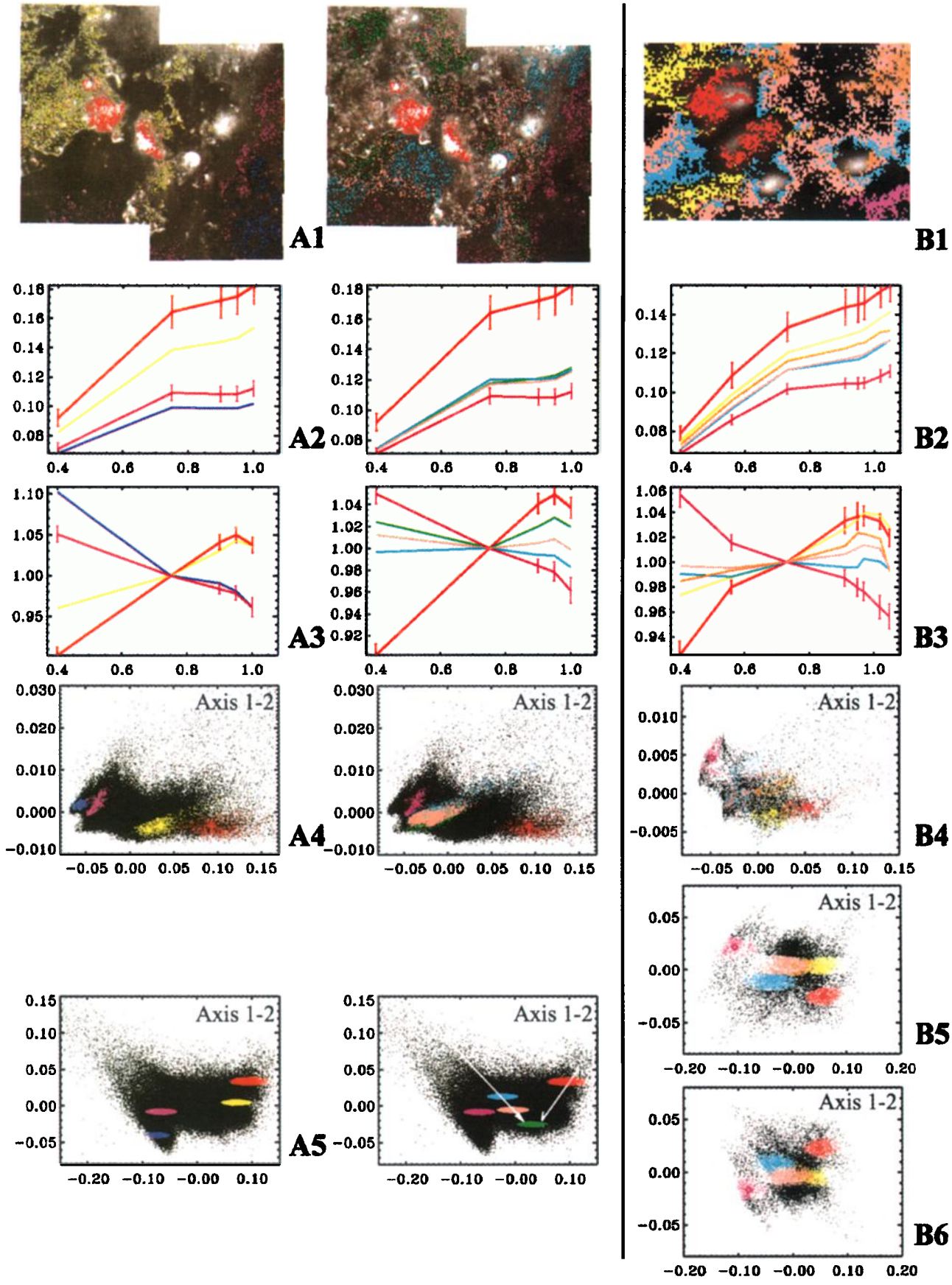

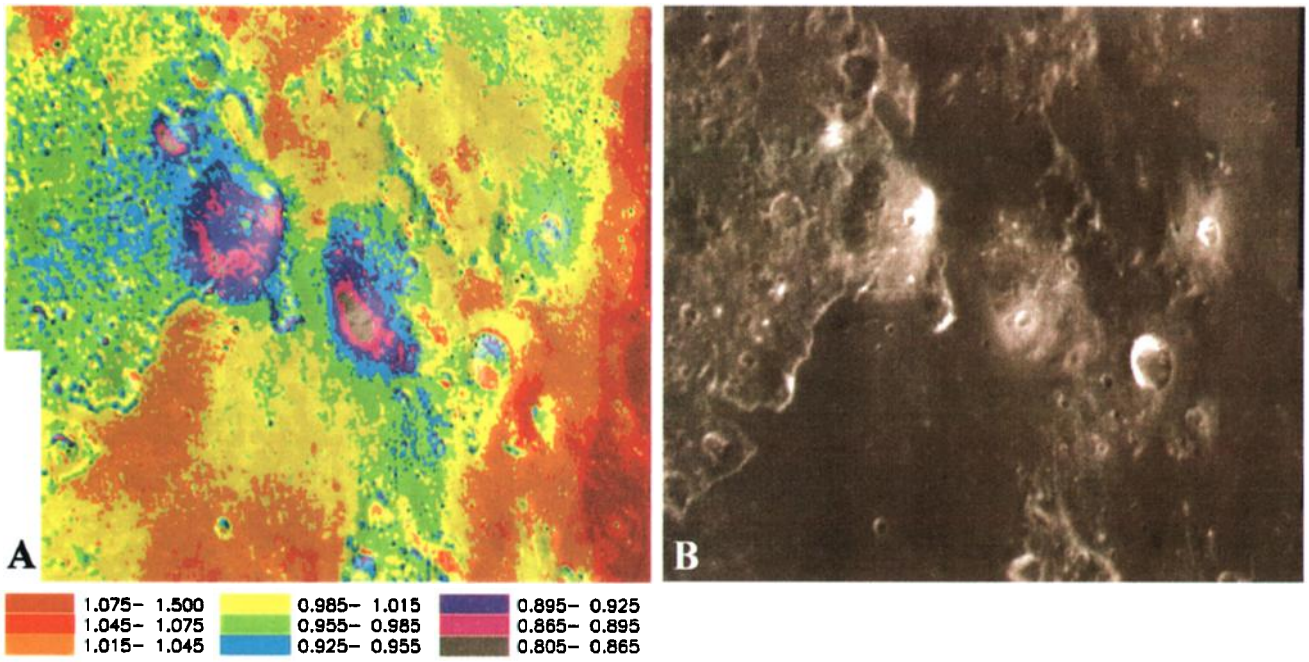

Plate 2. (a) Clementine 400/750 nm spectral ratio image relative to MS2, produced from the analyzed Clementine data set (see section 3), overlain on an oblique Clementine view of the Gruithuisen domes (see Plate 2b), in order to emphasize the relationships between observed spectral variations and surface morphology. Class interval for the ratio values is 3%. Color coding for this image is specific and does not relate to color coding used in other Plates herein this paper. (b) Corresponding Clementine image taken at 750 nm under 75° of phase angle, revealing the detailed morphology of the domes (resolution in meter per pixel, 150 along track and 230 a cross track).

1991; *Jaumann*, 1991; *Erard et al.*, 1993; *Cloutis*, 1996], PCA can be used to highlight mineralogical variations.

The PCA analysis is shown in Plate 1 for both the Clementine mosaic and the telescopic image. In Plate 1, A1 to A5 refer to the Clementine mosaic (for the sake of clarity, the analysis of the mosaic is displayed in two columns) and B1 to B6 refer to the telescopic image. PCA clouds are represented here in both absolute reflectance (reflectance PCA diagram; Plate 1, A4 and B4) and scaled reflectance (scaled PCA diagram; Plate 1, A5, B5, and B6). The use of these two kinds of PCA diagrams permits a better understanding of the main contributions arising from either reflectance continuum or absorption bands occurring in a specific wavelength domain [*Pinet et al.*, 1995; *Martin et al.*, 1996]. As a matter of fact, the consideration of the scaled reflectance data emphasizes the spectral slope influence versus the albedo, and we may gain some insight into the main spectroscopic contributions.

The PCA analysis we applied uses centered coordinates for both the absolute and scaled reflectance data, that is the (0,0) coordinates in all the Clementine and telescopic PCA diagrams in Plate 1 correspond to the barycenter point for the population. Since the uncertainty in the absolute reflectance estimates from (1) translates to the whole population of spectra through the linear regression, the analyses carried out in the PCA are quite appropriate, as they exhibit relative variations in the absolute reflectance data. Indeed, the PCA absolute and scaled reflectance scatter diagrams shown in Plate 1 are quite consistent for the telescopic and Clementine data sets. However, for the scaled reflectance data, a reverse pattern is noted for the telescopic PCA plot relative to the Clementine one (compare A5 and B5 in Plate 1). This difference arises from the spectral band available at 1050 nm for the telescopic data set, suggesting that this band bears a significant amount of information. Plate 1, B6 represents the PCA scaled diagram of the telescopic data set after removal of the 1050 nm spectral band. It shows that PCA scatter diagrams are quite consistent when one compares telescopic versus Clementine compatible data sets (i.e., selecting, in the telescopic data, the five wavelengths, 400, 730, 910, 980, and 1020 nm).

Introducing a method derived from the maximum likelihood classification technique, we use the notion of topological neighborhood in principal component (PC) space for setting a supervised classification process, emphasizing the identification of the extreme spectral types, their associated spatial distribution, and the possible mixing trends (each spectrum retrieved from the image cube is located as a single point in the PC space). This statistical analysis permits the derivation of a spectral classification with its related spatial distribution in the image [*Chevrel et al.*, 1995].

In absolute reflectance, the first three principal axes of variation (axis 1, 2, and 3) bear 98.7%, 0.6%, and 0.3%, respectively of the spectral variance for the telescopic data set (eight bands), and 99.1%, 0.7%, and 0.1% of the spectral variance for the Clementine data set (five bands). In scaled reflectance, variations along the three axes 1, 2, and 3, are 84.8%, 6.2% and 3.6%, and 84.9%, 12.9%, and 1.4%, for the telescopic and the Clementine data set respectively. This indicates that the dimensionality of the telescopic data set, analyzed in terms of spectral slope, is equal to 3 while the Clementine data set can be approximated by a projection in

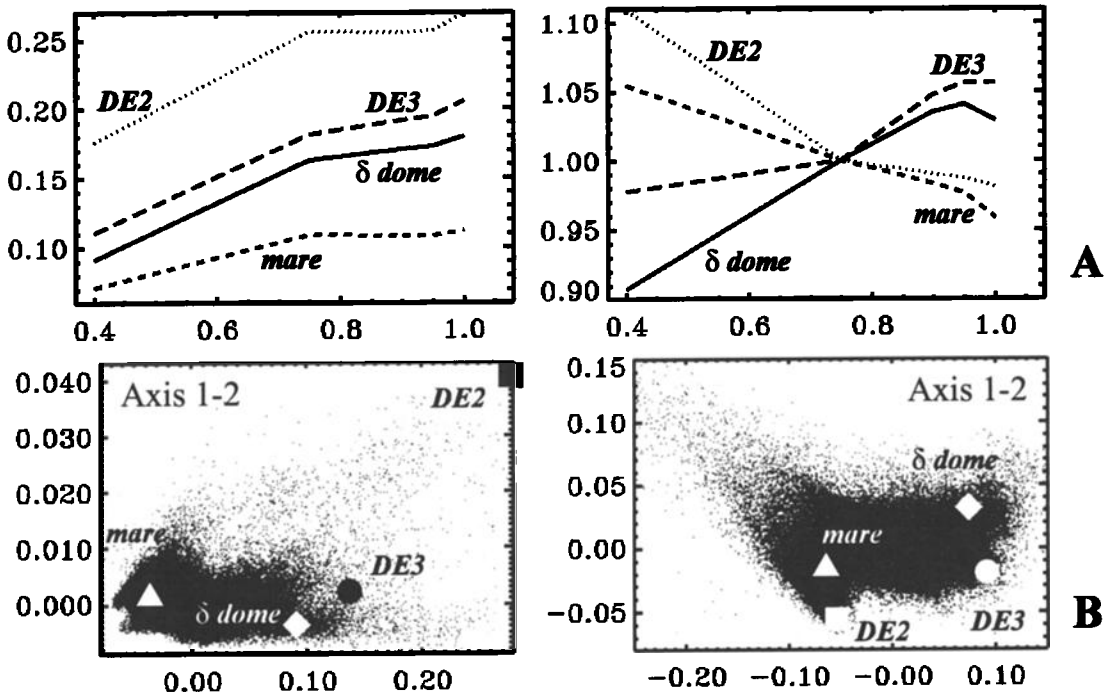

Figure 4. (a) Mean spectra of the dome and the mare unit (as in Figure 2a) plotted together with two external spectra [from *McCord et al.*, 1972] of highland lunar regions, Descartes 2 (DE 2) and Descartes-3 (DE 3), respectively corresponding to bright crater and background (i.e., mature) highland materials, showing (left) reflectance spectra and (right) relative to MS-2 reflectance spectra, scaled to unity at 750 nm. (b) Absolute (left) reflectance PCA diagram and (right) scaled PCA diagram for the two principal components (axes 1 and 2).

the plane of the first two axes. This means that a clear gain in spectral information is retrieved when considering eight bands instead of five in the visible near-infrared domain. The better definition of the spectral characteristics from the telescopic data is used for establishing the spectral classification. However, since more than 90% of the total variance is distributed along axes 1 and 2 and since we focus on the Clementine mosaic in the following discussion, we used mainly the PCA diagram corresponding to a projection of the data cloud in PC space along axes 1 and 2 (axis 1 in abscissa) to visualize the subsetting of the data cloud in relation to the definition of the spectral units. Accordingly, the PCA diagrams displayed herein correspond to a projection of PC space in the first principal planes defined by axes 1 and 2. The spectral units are identified in the multidimensional PC space on the basis of their topological homogeneity and clustering. The associated domains have been selected according to a neighboring topological sphere having a radius such that the deviation within the subpopulation of spectra considered does not exceed 3-5% in reflectance and 1% in relative reflectance to MS2 for every considered wavelength. The adopted deviation values relate to the level of coherency and the repeatability within the telescopic image and the Clementine mosaic for which the discrepancies at the boundaries of the overlapping frames are about 0.5% or less, depending on the considered wavelength. For each cluster selected in the cloud, the mean spectrum is shown in absolute reflectance (Plate 1, A2 and B2) and in relative reflectance to MS2 (Plate 1, A3 and B3) for highlighting the different spectral types. As shown in Plate 1 (A1 and B1), the corresponding spatial distribution of the associated homogeneous spectral units is produced for the Gruithuisen region. The resulting classification emphasizes the most extreme spectral behaviors.

5. Results

Several spectral units have been defined from the PCA analysis, corresponding to a dome unit, a dome-like unit, and mare units. These units, shown in Plate 1 in red (dome), yellow (dome-like), and violet/dark, blue/light, blue/pink (mare), are discussed in this section.

As noted, the clustering patterns on the reflectance PCA diagrams for both the Clementine (Plate 1, A4) and the telescopic (Plate 1, B4) images are similar. Also, the scaled PCA diagrams (Plate 1, A5, B5, and B6) do not differ greatly, and the relative location of the defined clusters is nearly the same in the PC space for both data sets. However, differences in the shape of the statistical clouds arise from (1) the difference in the coverage, (2) the difference in number of bands, and (3) the slight absolute reflectance difference. As a consequence, the mean spectra, shown in Plate 1, associated with clusters established from the two multidimensional data sets are not directly comparable and may present minor differences. However, the spatial distributions associated with these clusters are very consistent (see Plate 1, A1 and B1). In PC space, the first principal component appears mainly related to the albedo. Indeed, we notice an increase in the albedo for the spectra when one scans horizontally across the reflectance PCA diagram, i.e., from the mare unit (dark blue and violet) toward the dome unit (red)(Plate 1, A4 and B4). These two units exhibit extreme spectral shapes with the

lowest and the highest UV/VIS ratio for the dome (red) unit and the mare (dark blue and violet) units, respectively (Plate 1, A3 and B3). The second principal component is sensitive to variations in the spectral slope in the UV and the NIR domains. Details of the trends in terms of spectral variations observed within the PCA diagrams are discussed below.

In Figure 4a, spectra of the mare unit (h2 GS-3 type [*Pieters*, 1978]) and the Delta dome [*Head and McCord*, 1978] taken within the Clementine image are plotted (in absolute reflectance at left and relative to MS2 at right) along with two lunar highland spectra taken outside the image scene among spectra representative of highlands units [*McCord et al.*, 1972]. Two spectra are considered which correspond to (1) a bright highland crater material, from Descartes 2 (DE 2), and (2) a background (i.e., mature) highland material, from Descartes 3 (DE 3). Plots of the spectra (Figure 4a) in the statistical clouds of the Clementine mosaic indicate that there is no significant spectral contribution of highland material in the scene (see Figure 4b).

5.1. Red (Dome) Unit

The red spectral unit selected from the PCA diagram (Plate 1, A1 and B1) coincides with the Delta, Gamma, and NW domes (see Figure 1). It approximately outlines their morphological boundaries as mapped by *Head and McCord* [1978]. Spectral variations in this unit are less than 6% in albedo and less than 1% in reflectance relative to MS2. The reflectance spectrum for this unit typically shows a strong positive slope in the UV VIS domain (400-750 nm)(red spectrum in Plate 1, A2 and B2), indicating an absorption in the UV for the surface material corresponding to the domes. The reflectance spectrum relative to MS2 also displays a strong positive UV VIS slope (red spectrum in Plate 1, A3 and B3) and shows very low 400/750 nm relative (to MS2) ratio values of about 0.90 (see also Plate 2). The spectrum shows also a positive inflection (relative to MS2) in the NIR domain between 900 and 950 nm. This bumpy shape is better characterized with the more spectrally documented telescopic spectrum between 910 and 1050 nm. For the red unit, spectral variations in the NIR domain are less than 1%. Most of the variations for this unit are thus observed in the UV VIS domain (UV VIS slope). Furthermore, the telescopic data reveal that these slope variations are restricted to the 400-560 nm domain, indicating that the absorption feature in the UV is not large and is located shortward of 560 nm (Plate 1, B3). If we look closely at the spectral variations within the domes, it is found that the Delta dome and the Northwest dome are spectrally similar to each other and more homogeneous than the Gamma dome (the 400/750 nm relative to MS2 ratio is between 0.86 and 0.93 for the domes; see also Plate 2). The red unit (Plate 1, A1 and B1) does not correlate with the brightest parts of the domes, which correspond to relatively fresh craters [*Schultz*, 1976; *Head and McCord*, 1978]. These high albedo local areas on the domes appear spectrally much more heterogeneous (up to 8%) and show the lowest UV/VIS ratios relative to MS2 in the image (400/750 nm ratio < 0.85)(Plate 2).

5.2. Yellow (Dome-Like) Unit

The yellow unit (Plate 1, A1) is widespread across the image. Spectral variations within this unit for the Clementine data set are less than 6% (4.5% for the telescopic data set) in albedo and less than 0.8% (1.1% for telescopic) in reflectance relative to MS2. Morphologically, the yellow unit corresponds to hummocky upland regions near the domes (i.e., the red unit discussed before) and indeed partly surrounds them. It extends to the west and north of the domes within relatively high albedo areas. It was previously mapped (Figure 1a) as highland terrains dominated primarily by Iridum ejecta deposits [*Scott and Eggleton*, 1973; *Head and McCord*, 1978]. However, the present detailed spectral survey does not detect any significant highland-like component in the scene (see Figure 4). Small massifs embayed by mare material, north of the Delta and Gamma domes and south of the Delta dome, also belong to this unit (Plate 1, A1 and B1). The general spectral characteristics of the yellow unit are close to those of the red unit previously discussed. Indeed, the overall shape of the yellow unit mean spectrum (yellow spectrum in Plate 1) is very similar to that of the red unit. In the NIR domain, the shape of the inflection (relative to MS2) between 900 and 950 nm persists (Plate 1, A3 and B3). With respect to the red unit, we note a flattening of the positive UV VIS slope relative to MS2. This decrease in the UV VIS is indeed observed in the 400-560 nm spectral domain (see Plate 1, B3).

A clear change occurs in the spectral behavior (relative to MS2), both in the UV and in NIR domains, between the red/yellow units and the Imbrium mare units (violet and dark blue) located east of the domes (Plate 1, A1 and B1)(note that the dark blue unit falls outside the telescopic image). In the NIR domain, we observe for the mare units a negative slope (compare the red/yellow and the violet/dark blue spectrum in Plate 1, A3 (left) and B3. In the UV domain, the mare units (in violet/dark blue) are characterized by a negative UV VIS (400-730 or 750 nm) slope while the red and yellow units are characterized by a positive slope (Plate 1, A3 and B3). The additional band at 560 nm in the telescopic image shows more precisely that the 400-560 nm slope is positive for the yellow unit and negative for the violet mare unit (Plate 1, B3). These spectral characteristics indicate that the material of the yellow unit is spectrally different from the surrounding mare material, its spectral properties being closer to those of the dome materials (red unit). In the following, the yellow unit (Plate 1) is referred to as the "dome-like" unit. Examination of the Lunar Orbiter image IV-151-H2 (Figure 1b) and the Apollo 15 image (Figure 1c) shows that the yellow unit mainly corresponds to moderate to relatively high topographic features, e.g., the rugged terrains lying west of the Gamma dome, the topographic high NW-SE trending massif located north of the Delta dome (branch-shaped massif, noted "br" in Figure 1b), and also the branch-shaped terrain located east of mare patch P (see Figure 1b).

The more spectrally documented telescopic data set splits this dome-like unit into two subunits: a yellow unit surrounding the domes and an orange unit located north of the domes (Plate 1, B3). This orange unit, though displaying the same spectral characteristics, exhibits a less pronounced bump at 1μ, with a strong decrease toward 1050 nm (between 1020 and 1050 nm, the decrease is 3% and 1.5% for the orange and the yellow unit, respectively; compare the yellow and orange spectra in Plate 1, B3), responsible for the discrimination of this subunit.

5.3. Violet, and Dark and Light Blue (Mare) Units

Domains represented by violet, dark blue and light blue colors in the PCA diagrams (Plate 1) coincide with the low albedo areas in the image. They correspond morphologically

to mare regions, i.e., the border of Mare Imbrium and mare patches embaying the domes region. Dispersion within the spectra for the mare violet, dark blue, and light blue units is less than 4% in reflectance and 1% in relative reflectance to MS2 for the Clementine data set (3% and 1%, respectively, for the telescopic one). The violet unit (Plate 1, A1 and B1) corresponds to the border of Mare Imbrium. Its mean spectrum is very close to the mare spectrum of hDSA type [*Pieters*, 1978], and indeed the mare reference for this spectral type is located within this unit (see Figure 2). The dark blue mare unit corresponds to the extreme eastern portion of Mare Imbrium in the Clementine image (Plate 1, A1 (left)) (this portion of Mare Imbrium is not included in the telescopic image). The light blue mare unit corresponds to mare areas located (1) immediately south of the Delta and Gamma domes (and also in the "channel" between them), (2) at the boundary of Mare Imbrium and around the crater Gruithuisen B (GB in Figure 1b), and (3) around a small crater located north of Gruithuisen B.

As noted, the mare units are spectrally characterized (relative to MS2) by a negative slope in the NIR domain and by a positive UV-VIS slope. Values of the UV / VIS ratio are 1.10 and 1.05 for the dark blue and the violet units, respectively (Plate 1, A3). The light blue unit has spectral characteristics very close to those of the MS2 area (Mare Serenitatis), as its relative spectrum to MS2 is almost flat (Plate 1, A3 (right) and B3).

5.4. Intermediate Spectral Domains

From this PCA analysis (Plate 1), two kinds of domains have been identified within the PC space, corresponding to extreme spectral types a and b. These domains are spatially represented by homogeneous spectral units morphologically corresponding to the Gruithuisen domes and their surroundings (type a) and the mare units (type b). The red (dome) and yellow (dome-like) units are spectrally characterized (relative to MS2) by a positive UV / VIS slope and a "bumpy" shape (values > 1.00) in the NIR domain (Plate 1, A3 and B3). Spectral differences between the red and yellow units occur mainly in the UV / VIS slope (see Plate 1, A3 (left)). Domains corresponding to these units occupy the rightmost portion of the PCA-scaled (axes 1 and 2) diagram (Plate 1, A5). The violet and dark blue units correspond to mare units located east and south of the domes, i.e., to the border of Mare Imbrium. These two units are spectrally characterized (relatively to MS2) by a negative UV / VIS slope and a small bumpy shape (values < 1.00) in the NIR domain (Plate 1, A3). Spectral differences between these two units also occur in the UV / VIS slope (see Plate 1, A3 (left)). Domains corresponding to these units occupy the leftmost portion of the PCA-scaled (axes 1 and 2) diagram (Plate 1, A5).

Exploration in PC space, in the particular projection (axes 1 and 2) of the data cloud in Plate 1, A5 and B5, shows intermediate spectral behaviors between type a and b. Three clusters have been selected for highlighting this possible evolutionary trend, referred as the light blue, pink and green clusters, shown in plate 1, A4 and A5 (right) along with the clusters corresponding to the domes (red) and the mare (violet) units. Their corresponding spatial distribution in the image is shown in Plate 1, A1 (right). The light blue, pink, and green clusters display closely similar spectral characteristics, the differences in reflectance relative to MS2 being less than 2% and 4% in the UVVIS and NIR domains, respectively (Plate 1, A3 (right), and B3).

These three clusters do not necessarily define true additional spectral units within the population of spectra. The simplest explanation for these clusters is that they represent variations in the composition and stratigraphic exposure of several different mare units and subunits (R. J. Wagner et al., manuscript in preparation, 1998). They may, however, show that in some cases a gradational change in the spectral behavior between the dome-like and mare-like materials exists. Such a spectral change could arise from a gradational compositional change and/or might be related to a spatial mixing between different types of terrains. The spatial distribution in the image for the light blue, pink, and green domains corresponds to relatively low to intermediate albedo areas (Plate 1, A2 and B2), i.e., mare regions (Plate 1, A1). As noted previously, the light blue unit shows spectral characteristics close to those of the standard area MS2 in Mare Serenitatis (Plate 1, A3 (right) and B3), and its spatial distribution is described in section 5.3 relative to the mare units. Spatially, the pink domain appears as an extension of the light blue unit. It mainly corresponds to the mare patches embedded in the yellow unit located north of the domes (Plate 1, A1 and B1). In fact, the areas mapped in light blue or pink appear to be adjacent to the yellow (dome-like) unit (Plate 1, A1 and B1). The green domain (Plate 1, A1 (right)) displays distinctive spectral characteristics (relative to MS2), with, on one hand, the presence of a bump in the NIR (which characterizes the dome and the dome-like spectral domains (however, the bump is 2-3% lower than for the dome/dome-like)), and, on the other hand, a negative UV / VIS slope (which characterizes the mare spectral domains (the value of the UV / VIS ratio being 1.02))(see Plate 1, A3 (right)). These spectral characteristics appear to be intermediate between those displayed by the dome-like and the mare materials. Although these spectral features are not extreme, they may be significant and could define a separate spectral unit, as the green cluster is on the edge of the cloud in the PCA-scaled (axes 1 and 2) diagram (plate 1, A5 (right)), at the intersection of two spectral (mare-like and dome-like) trends, shown by white arrows in plate 1, A5 (right). Furthermore, the green cluster corresponds to a coherent spatial unit (mare patch noted P in Figure 1b) and to the southern portion of another mare patch located east of mare patch P. This suggests the existence of a distinct mare subunit as well as a gradational spectral change or a mixing between the materials of the dome-like (yellow) and the mare (violet) materials. As already noted, the yellow, light blue, pink, and green domains display a spatial organization, as they are embaying the yellow unit (see Plate 1, A1), suggestive of mare subunits.

6. Interpretation and Discussion

6.1. Dome Unit

Before this study, only two reflectance spectra were available, taken at low spatial resolution on the Delta and the Gamma domes, and it was recognized that these spectra typically show the properties of high-albedo lunar regions known as red spots [*Head and McCord*, 1978]. The red unit displayed in Plate 1 has the spectral characteristics of red spots. This unit, which corresponds to the area outlined by the morphological limits of the domes, can therefore be regarded

as a unit (dome unit) representing dome material and having the spectral characteristics of red spots. The mean spectrum associated with the red domain in the PCA diagrams (plate 1) may be representative of the general spectral properties of red spots. Beyond the obvious strong positive UV VIS slope noted owing to a strong absorption in the UV, significant changes are observed in the UV VIS slope which appear to be responsible for the spectral heterogeneities within the dome unit and particularly within the Gamma dome. The cause of these spectral heterogeneities is not determined presently. They might be due to optical effects (such as soil maturation processes) and/or compositional differences (such as TiO_2 content or differences in mineralogical abundances). At the present time, the spectral characteristics of the lunar red spots are still poorly understood in terms of mineralogy and/or lithology. The cause of the strong absorption in the UV is not clearly determined, and very few interpretations have been advanced. From analysis of early reflectance spectra (400-780 nm) [*McCord et al.*, 1972], *Malin* [1974] inferred a composition similar to those of Apollo 14 soils for the red spots, i.e., mature soils with high glass content and low-calcium pyroxene (orthopyroxene). On the basis of Al/Si and Mg/Si ratio, *Malin* [1974] also suggested a KREEP composition for the red spots. However, the Apollo X ray fluorescence experiment did not overfly the Gruithuisen domes region. According to *Head and McCord* [1978], the spectral characteristics of red spot areas might indicate that these areas are covered with mature (agglutinate rich) soils with a lower content of iron and titanium than mare soils and most highland soils. The Gamma dome is topped by two small impact craters with high albedo ejecta (Figures 2b and 2c and Plate 2b). Spectra for these craters display the strongest UV VIS slope within the domes (400/750 nm ratio relative to MS2 is equal to 0.83)(Plate 2a) and a marked decrease in reflectance toward 1000 nm. It is likely that these craters have exposed locally fresh dome material and the related observed spectral variations are attributed to optical effects. Besides, some of the observed spectral heterogeneities (see Plate 2a) are clearly associated with morphological units on the domes, such as lava flows mapped by *Head et al.* [1978]. It is worth noting the crescent-like shape of these heterogeneities seen on the flank of both Gamma and Delta domes, which could be suggestive of nonexplosive eruption of lava (see Plate 2b). These differences would result from differences in composition and/or from a variable surface proportion of crystalline exposed rocks versus glass-rich or pumiceous materials as seen on terrestrial silicic domes [*Eichelberger et al.*, 1986]. However, we cannot rule out the possibility that these flow units on the slopes of the domes might also be interpreted as landslides having exposed fresh dome material.

6.2. Mare Units

The mean spectral characteristics of the light blue mare unit are very close to those of MS2 in Mare Serenitatis. According to the empirical calibration of telescopic 400/730 nm ratio values (relative to MS2) to weight percent TiO_2 from *Johnson et al.* [1991b], this gives a TiO_2 weight percent value of 1 to 2.5 for this unit, corresponding to very low to low TiO_2 basalts [*Neal and Taylor*, 1992]. The spectral characteristics of the violet (Plate 1, A3 and B3) and the dark blue unit (Plate 1, A3, not mapped in the telescopic image) are close to each other in the NIR domain. They differ only in regard to the 400/750 nm spectral ratio relative to MS2, ranging from 1.03 to 1.05 and from 1.07 to 1.10 (for the violet and dark blue units, respectively) (Plate 1, A1 and Plate 2). The corresponding TiO_2 weight percent values ranges from about 3% to 4-6% for the basalts forming these two Imbrium mare units [*Johnson et al.*, 1991b]. These values are consistent with those given by *Johnson et al.* [1991a] in the TiO_2 abundance map for the nearside lunar maria, given the differences in spatial resolution existing between this map (about 5.3 km/pixel) and the present Clementine coverage. The mare basalts for the violet and dark blue units (Plate 1, A1) thus correspond to low to medium TiO_2 basalts according to the mare basalt classification [e.g., *Pieters* 1978; *Neal and Taylor*, 1992]. These two mare units appear to be fairly spectrally homogeneous throughout their area (see Plate 2).

6.3. Yellow (Dome-Like) Unit

Clearly, the yellow unit is spectrally close to the dome (red) unit and differs from the surrounding mare units. However, the spectral characteristics of its material neither resemble those of fresh nor background highland materials (Figure 4). In Plate 1, A3 and B3, if we look at the UV VIS spectral domain only, the trend in the UV / VIS slope from the dome spectrum (in red) to the mare spectra (light blue, violet, and dark blue) might suggest, for the material constituting the yellow unit, a possible contamination by mare material or a possible progressive combination of both types of dome and mare materials. However, the positive UV VIS slope revealed by the additional 560 nm band in the telescopic image for the yellow unit indicates that this unit has a different spectral behavior than the mare units (Plate 1, B3). Local contamination of the yellow unit material by mare materials is possible, as local mare patches occur within the yellow unit. As noted, the pink and/or green areas in plate 1, A1, might represents such a mixing. We also cannot rule out a contamination or combination of dome material with some background materials. In the Gruithuisen region, background materials are made of highland material and Imbrium basin deposits represented by the Fra Mauro Formation and/or the Cayley Formation [*Spudis et al.*, 1988], followed by ejecta (highland and Imbrium ejecta) deposits from the Iridum event [*Head and McCord*, 1978], which are widespread in this area. However, it has been shown that the contribution of highland material (such as DE 2 and DE 3) should be very limited, if any (Figure 4). It is suggested that the dome-like (yellow) unit likely represents Iridum material mixed or contaminated with dome (red) material. Whatever the presence and the nature of possible contaminant materials, the spectral characteristics of the yellow unit suggest it contains a significant proportion of dome material.

Although the spectral characteristics of the dome material are not explained in terms of composition at the present time, it nonetheless appears that this material is present in significant proportions in a large area outside the morphological boundaries of the domes, in the yellow unit in Plate 1, A1 and B1. Plate 2a points out the widespread distribution of the unit with dome-like spectral UV / VIS characteristics in relation to the local morphology. It suggests that the specific style of eruption that is inferred for the formation of the domes, i.e., high viscous flows of possible more silicic composition [*Head et al.*, 1978], might have occurred over a large regional scale in this part of the

Moon. This observation is supported by the fact that other similar volcanic features, the Mairan domes [*Wood and Head*, 1975; *Head and McCord*, 1978; *Head et al.*, 1978], exist in this region, about 200 km northwest of the Gruithuisen domes (see Figure 1a). The dome-like unit we identified extends northwest and north of the Gruithuisen domes, toward the Mairan dome region (Plate 1, A1).

The Gruithuisen domes predate the surrounding mare surfaces [*Malin*, 1974]. Ages of 3.3 to 3.6 Ga and 3.2 to 3.3 Ga were previously inferred for the domes and the surrounding mare deposits, respectively [*Head and McCord*, 1978]. However, recent measurements of crater size-frequency distribution indicate ages of 3.72-3.80 Ga for the domes, ages of 3.30-3.55 Ga for the oldest, and 3.0 Ga (and younger) for the youngest mare units [*Wagner et al.*, 1996]. These ages for the domes (the earlier part of Late Imbrian) [*Wagner et al.*, 1996] are older than previously thought and indicate that the domes are not contemporaneous with most of the mare deposits surrounding them. They appear to have formed before the major episode of basin flooding on the Moon by effusive lavas emitted at high eruption rates.

Formation of the domes occurred at a time of extensional horizontal surface stress in lunar history, which encouraged ascent and eruption of magma [*Solomon and Head*, 1979], particularly along important fractures resulting from basin formation. The extensional context at this time may help to explain the setting of the Gruithuisen domes at the edge (on top of the intermediate (second) ring) of the Imbrium basin.

The morphology of the Gruithuisen domes is consistent with viscous magmas of more silicic composition than basalt [*Head et al.*, 1978]. We know that on Earth, appreciable quantities of highly silicic magma are produced by the chemical evolution of basaltic magma bodies stored in shallow crustal reservoirs and that this process is not itself controlled by the tectonic environment in which it takes place (i.e., extensional or compressional).

The eruption of volatile-bearing silicate-rich magmas, which is commonly very explosive on Earth, is expected to be even more extreme on the Moon because of the external environment [*Wilson and Head*, 1981]. Consequently, if magmatic disruption occurred during the emplacement of the domes, the products of these explosive eruptions (pumiceous pyroclasts) should be so fine grained and widely dispersed that they should produce no positive construct around the vent and no well-defined ejecta deposit [*Wilson and Head*, 1983]. This could account for the wide areal extent of a dome-like material component around the domes. Under these conditions, the pyroclastic material may have been emitted from the domes themselves or from other source vents located within the dome-like unit. This scenario would imply the presence of sufficient volatiles in the magma to cause disruption. However, it is also possible that the formation of the Gruithuisen domes results from viscous magmas extruded at lower extrusion rates than mare basalts. In this case, flows such as the ones observed in association with Gruithuisen Gamma [*Head et al.*, 1978] may have resurfaced the surrounding areas. Source vents for such flows may have also occurred within the dome-like unit, as well as in the dome region. The presence and the volumetric importance of the Delta, Gamma, and NW domes might be due to their position on top of the Imbrium ring fractures which might have also favored the supply of magmas for a longer time span. In any case, the wide distribution of the dome-like materials and the preliminary morphological identification of an unknown dome-like feature modified by Iridum crater ejecta (Figure 1b, just north of br) suggest that dome formation had commenced prior to the Iridum impact event and that this unit was more widespread than suggested by the post-Iridum morphological domes.

A key point for further studies in the understanding of the volcanic history of this region is the definition of the real spatial extent and the limits of the dome-like unit and particularly the determination of whether there is a relation between the Gruithuisen and Mairan dome complexes (Figure 1a) through a unit such as the dome-like unit. On the basis of morphological studies, we also need to determine more precisely the relations (surface mixing, distribution, and stratigraphy) within the dome-like unit, and between the dome-like material and the background material (Imbrium and Iridum ejecta) and/or local patches of mare material [J. W. Head et al., manuscript in preparation, 1999].

7. Conclusions

This work represents an improvement in the determination of the spectral characteristics of red spot spectra and the characterization of the spatial extent of the three (Delta, Gamma and NW) Gruithuisen domes (dome unit in red in Plate 1). Their general spectral characteristics are a strong UV VIS slope corresponding to 400/750 nm relative to MS2 ratio values ranging between 0.83 and 0.93 and the presence of a bumpy shape (relative to MS2) in the NIR around 900-950 nm. The spectral variability existing within the domes, mainly observed in the UV VIS domain between 400 and 560 nm, may be due to optical and/or compositional surface effects and be indicative of the presence in variable surface proportion of crystalline exposed rocks versus glass-rich areas, as seen on terrestrial silicic domes.

Two distinctive mare basalt units are identified. The mare unit surrounding the domes is characterized by very low to low TiO_2 contents (about 3 wt%), while the mare unit located deeper within Mare Imbrium shows low to medium TiO_2 content values (3 to 6 wt%) [*Neal and Taylor*, 1992].

Embaying the dome units and extending into their surroundings in relatively high albedo areas previously mapped as highland terrains, we mapped a widespread unit referred here as the dome-like unit (yellow coding in Plate 1). This dome-like unit presents spectral characteristics close to those of the dome unit material (red spot), and this, together with evidence of a pre-Iridum dome, suggests that the dome unit might be much more widespread in this region (Plate 2) prior to the Iridum impact event. It suggests that the specific style of eruption which is inferred for the formation of the domes, i.e., viscous flows of possible more silicic composition [*Head et al.*, 1978], might have occurred over a large regional scale in this part of the Moon.

This region of the Moon shows very unusual spectral characteristics and, given its spatial extent, should be a target of particular interest to be characterized by the geochemical survey planned by the Lunar Prospector set of spectrometers, as it could tell much about earlier stages and ancient styles of the lunar volcanism. In particular, this will give some additional constraints about the inferred composition of the Gruithuisen domes and the lunar red spots (e.g, silicic [*Head et al.*, 1978], KREEP [*Malin*, 1974] composition).

Acknowledgments. This research was funded by the French "Programme National de Planétologie" (PNP), INSU, CNRS (SDC and PCP), and NASA grant NAGW-2185 (J W.H.). The authors are grateful for the numerous helpful comments of the two referees, J. Johnson and B. R. Hawke, whose contributions significantly improved the paper. We also thank J. Sunshine for the help she provided for the projection of the telescopic images onto digitized Lunar Orbiter photographs while visiting the Department of Geological Sciences at Brown University, F. Bellagh and Y. Daydou at the Geoscience computer facilities at Midi-Pyrénées Observatory (Toulouse), and GRGS/CNES for its support in computational facilities.

References

Bruno, B. C., P. G Lucey, and B. R. Hawke, High-resolution UV-Visible spectroscopy of lunar red spots, *Proc. Lunar Planet. Sci. Conf., 21st*, 405-415, 1991.

Chevrel, S. D. and P. C. Pinet, Revisited geology of Gassendi crater from Earth-based near-infrared multispectral solid state imaging, *Proc. Lunar Planet. Sci. Conf., 22nd*, 249-258, 1992.

Chevrel, S. D , P. C. Pinet, and J. W. Head, Exploration of the morphological distribution of the spectral units in the Gruithuisen domes region (abstract), *Lunar Planet. Sci., XXV*, 249-250, 1994

Chevrel, S. D., P. C. Pinet, J. W. Head, and F Bellagh, UV-VIS-NIR spectral classification in the Gruithuisen domes region (abstract), *Lunar Planet. Sci., XXVI*, 241-242, 1995.

Chevrel, S. D., P. C. Pinet, and J. W. Head, Gruithuisen domes region: A candidate for a large extended lunar nonmare volcanism unit (abstract), *Lunar Planet. Sci., XXVII*, 215-216, 1996.

Cloutis, E. A., Hyperspectral geological remote sensing: Evaluation of analytical techniques, *Int. J. Remote Sens., 17* (12), 2215-2242, 1996.

Davis, J. C., *Statistics and Data Analysis in Geology*, John Wiley, New York, 1973.

Eichelberger, J. C., C. R. Carrigan, H. R. Westrich, and R. H. Price, Non explosive silicic volcanism, *Nature, 323*, 598-602, 1986.

Erard, S., P. Cerroni, and A. Coradini, Automatic definition of spectral units in the equatorial regions of Mars (abstract), *Lunar Planet Sci , XXIV*, 443-444, 1993.

Gaddis, L. R., A. S. McEwen, and T. L. Becker, Compositional variations on the Moon: Recalibration of Galileo solid-state imaging data for the Orientale region and farside, *J. Geophys. Res., 100*, 26,345-26,355, 1995.

Greeley, R., et al., Galileo imaging observations of lunar maria and related deposits, *J. Geophys. Res., 98*, 17,183-17,205, 1993.

Hartmann, W. K., et al., Chronology of planetary volcanism by comparative studies of planetary cratering, in *Basaltic Volcanism on the Terrestrial Planets*, chap. 5, pp.1049-1127, Pergamon, Torrytown, N. Y., 1981.

Hawke, B. R., and J. F. Bell, Remote sensing studies of lunar dark-halo impact craters. Preliminary results and implications for early volcanism, *Proc. Lunar Planet. Sci. Conf., 12th*, 665-678, 1981.

Head, J. W., Lunar volcanism in space and time, *Rev Geophys , 14*, 265-300, 1976.

Head, J. W., and A. Gifford, Lunar mare domes: Classification and modes of origin, *Moon Planets, 22*, 235-258, 1980.

Head, J. W., and T. B. McCord, Imbrian-age highland volcanism on the Moon: The Gruithuisen and Mairan domes, *Science, 199*, 1433-1436, 1978.

Head, J. W., and L. Wilson, Lunar mare volcanism: Stratigraphy, eruption conditions, and the evolution of secondary crusts, *Geochim Cosmochim. Acta, 56*, 2155-2175, 1992.

Head, J.W., P. C. Hess, and T. B. McCord, Geologic characteristics of lunar highland volcanic (Gruithuisen and Mairan region) and possible eruption conditions (abstract), *Lunar Planet Sci , IX*, 488-489, 1978.

Head, J. W., S. L. Murchie, J. F. Mustard, C. M. Pieters, G. Neukum, A. McEwen, R. Greeley, E. Nagel, and M. J. S. Belton, Lunar impact basins: New data for the western limb and far side (Orientale and South Pole-Aitken basins) from the first Galileo flyby, *J. Geophys. Res., 98*, 17,149-17,181, 1993.

Jaumann, R., Spectral-chemical analysis of lunar surface materials, *J. Geophys. Res., 96*, 22,793-22,807, 1991.

Johnson, J. R., S. M. Larson, and R. B. Singer, Remote sensing of potential lunar resources, 1, Nearside compositional properties, *J Geophys. Res., 96*, 18,861-18,882, 1991a.

Johnson, J. R., S. M. Larson, and R. B. Singer, A revaluation of spectral ratios for lunar mare TiO_2 mapping, *Geophys. Res. Lett.,18*, 2153-2156, 1991b.

Johnson, P. E., M. O. Smith, and J. B. Adams, Quantitative analysis of planetary reflectance spectra with principal component analysis, *Proc. Lunar Planet. Sci. Conf., 15th*, Part 2,, *J. Geophys. Res., 90*, suppl., C805-C810, 1985.

Johnson, P. E., P. C. Pinet, and S. D. Chevrel, Multispectral mixture modeling of the Apollo 15 landing site, in *Actes Colloque National de Planétologie, Vol 2*, pp. S8-51, *Univ. Paul Sabatier, Toulouse, France*, 1994.

Kaydash V. G., and Y. G Shkuratov, Fe, Ti and IS/FeO maps for the lunar nearside: News estimations by optical data, *Proc. Lunar Planet. Sci. Conf., 29th*, 1089-1090, 1998.

Laughlin, W. P., Principal component analysis for alteration mapping, *Photogramm. Eng. Remote Sens., 28*, 295-304, 1991.

Lucey P.G., D.T. Blewett, and B.R. Hawke, Mapping the FeO and TiO2 content of the lunar surface with multispectral imagery, *J. Geophys. Res , 103*, 3679-3699, 1998.

Malin, M., Lunar red spots: Possible pre-mare materials, *Earth Planet. Sci. Lett., 21*, 331-341, 1974.

Martin, P. D., P. C. Pinet, R. Bacon, A. Rousset, and F. Bellagh, Martian surface mineralogy from 0.80 to 1.05 mm Tiger spectro-imaging measurements in Terra Sirenum and Tharsis Montes formation, *Planet. Space Sci., 44*, 859-888, 1996.

McCord, T. B., Color differences on the lunar surface, Ph.D. thesis, Calif. Inst. of Technol., Pasadena, 1968.

McCord, T. B., Time dependence of lunar differential color, *Astron. J., 74*, 273-278, 1969.

McCord, T. B., M. P. Charette, T. V. Johnson, L. A. Lebofsky, and C. M. Pieters, Lunar spectral types, *J. Geophys. Res., 77*, 1349-1359, 1972.

McCord, T. B., C. M. Pieters, and M. A. Feierberg, Multispectral mapping of the lunar surface using ground-based telescopes, *Icarus, 29*, 1-34, 1976.

McEwen, A. S., A precise lunar photometric function (abstract), *Lunar Planet. Sci., XXVII*, 841-842, 1996.

Müller, A., B. R Hawke, P. G. Lucey and C. M. Pieters, Remote sensing and geologic studies of the Lassell region of the Moon (abstract), *Lunar Planet Sci. Conf., XVII*, 577-578, 1986.

Neal, C R., and L. A. Taylor, Petrogenesis of mare basalts: A record of lunar volcanism, *Geochim. and Cosmochim. Acta, 56*, 2177-2211, 1992.

Nozette S , et al., The Clementine mission to the Moon: Scientific overview, *Science, 266*, 1835-1839, 1994.

Pieters, C.M , Mare basalts types on the front side of the Moon, *Proc. Lunar Planet Conf., 9th*, 2825-2849, 1978

Pieters, C. M., Composition of lunar highland crust from near-infrared spectroscopy, *Rev. Geophys., 24*, 557-578, 1986.

Pieters, C. M., et al , Crustal diversity of the Moon: Compositional analyses of Galileo solid state imaging data, *J. Geophys. Res., 98*, 17,127-17,148, 1993.

Pinet, P. C., S. D. Chevrel, and P. Martin, Copernicus. A regional probe of the lunar interior, *Science, 260*, 797-801, 1993.

Pinet, P. C , F. Costard, S. D. Chevrel, P. Martin, F. Bellagh and J. Blamont, Aristarchus plateau spectral mapping from Clementine and telescopic high resolution spectro-imaging data (abstract), *Lunar Planet. Sci , XXVI*, 1123-1124, 1995.

Pohn, H. A., and R L. Wildey, A photoelectric-photographic study of the normal albedo of the Moon, *U.S. Geol. Surv Prof Pap. ,599E*, 1970.

Sasaki, K., K. Satoshi, and S. Minami, Constrained nonlinear method for estimating component spectra from multicomponent mixtures, *Appl. Opt., 22*, 3599-3603, 1983.

Schultz, P. H., *Moon Morphology*, Univ. of Tex Press, Austin, 1976.

Schultz, P. H., and P D Spudis, Evidence for ancient mare volcanism, *Proc Lunar Planet. Sci. Conf., 10th*, 2899-2918, 1979.

Schultz, P. H., and P. D. Spudis, The beginning and end of lunar mare volcanism, *Nature, 302*, 233-236, 1983

Scott, D. H., and R. E. Eggleton, Geologic map of the Rumker quadrangle of the Moon, *USGS Geologic Atlas of the Moon, Map I-805, U. S. Geol. Surv., Washington D. C.* , 1973

Smith, E. I., Identification, distribution and significance of lunar volcanic domes, *Moon, 6*, 3-31, 1973.

Smith, M. O., S. L Ustin, J B Adams, and A. R. Gillespie, Vegetation in deserts, I, A regional measure of abundance from multispectral images, *Remote Sens. Environ., 31*, 1-26, 1990a.

Smith, M. O., S. L. Ustin, J. B. Adams, and A. R. Gillespie, Vegetation in deserts, II, Environmental influences on regional abundance, *Remote Sens. Environ., 31*, 27-52, 1990b.

Solomon, S., and J. W. Head, Vertical movement in mare basins: Relations to mare emplacement, basin tectonics, and lunar thermal history, *J. Geophys. Res., 84*, 1667-1682, 1979.

Spudis, P. D., B. R. Hawke, and P. G. Lucey, Materials and formation of the Imbrium basin, *Proc. Lunar Planet Sci. Conf., 18th*, 155-168, 1988.

Wagner, R. J., J. W. Head, U. Wolf, and G. Neukum, Age relations of geologic units in the Gruithuisen region of the Moon based on crater size-frequency measurements (abstract), *Lunar Planet. Sci., XXVII*, 1367-1368, 1996.

Whitaker, E A., Lunar color boundaries and their relationship to topographic features: A preliminary survey, *Moon, 4*, 348-355, 1972.

Wilhelms, D. E., The geologic history of the Moon, *U. S. Geol. Surv., Prof. Pap. 1348*, 1987.

Wilson, L., and J. W. Head, Ascent and eruption of basaltic magma on the Earth and Moon, *J. Geophys. Res., 86*, 2971-3001, 1981.

Wilson, L., and J. W. Head, A comparison of volcanic eruption processes on Earth, Moon, Mars Io and Venus, *Nature,* 663-669, 1983.

Wood, C. A., and J. W Head, Geologic setting and provenance of spectrally distinct pre-mare material of possible volcanic origin, *papers presented at the Conference on Origin of Mare Basalts*, Lunar Sci. Inst., Houston, Tex., 1975.

S. D. Chevrel and P. C. Pinet, Laboratoire de Dynamique Terrestre et Planétaire, UMR5562/CNRS, Groupe de Recherche de Geodésie Spatiale, Observatoire Midi-Pyrénées, 14 Av. E. Belin, 31400 Toulouse, France (Serge.Chevrel@cnes.fr)

J. W. Head, Department of Geological Sciences, Brown University, Providence, Rhode Island.

(Received May 28, 1997; revised August 12, 1998; accepted August 24, 1998.)